Radar Differential Phase Upon Transmission Impacts Products From Atmospheric Insects

Valery M. Melnikov[®], *Member, IEEE*, and Eli S. Bridge

Abstract—The U.S. network of WSR-88D dual-polarization weather radars adheres to design standards that are intended to ensure uniform radar measures from atmospheric phenomena. Although these radars have been designed to collect weather information, they also monitor atmospheric biota. In this communication, we demonstrate that radar patterns from airborne insects from co-located WSR-88Ds can differ significantly. We explain these discrepancies as a result of different phase shifts between transmitted polarized radar waves, and we argue that this phase is a critical radar parameter for the interpretation of radar variables from airborne insects.

Index Terms—Polarimetric radar, radar echoes from insects, radar measurements.

I. Introduction

EATHER radar networks allow for almost continuous data collection on a continental scale, and they are widely used for the observations of airborne animals to provide important information for ornithology, entomology, ecology, and agriculture [1], [2], [3], [4]. Central to the concept of radar networks is that uniformity among the individual radar stations gives rise to uniformity of observed radar variables, which makes it possible to build composite radar products that span multiple coverage areas [5], [6].

Several properties of airborne animals can be inferred from modern weather radars, including abundance, flight direction/velocity, and general species composition [1], [4], [7], [8], [9]. However, unlike hydrometeors, which produce consistent values for radar reflectivity (Z) and differential reflectivity (Z_{DR}) across radars, radar patterns from airborne animals, particularly insects, can differ across radar installations. To demonstrate these differences, we have collected data from co-located dual-polarization Doppler radars (i.e., Weather Surveillance Radar-1988, Doppler or WSR-88D, also known as NEXRAD) that show significant variations in the observed

Manuscript received 18 February 2024; accepted 29 February 2024. Date of publication 7 March 2024; date of current version 21 March 2024. This work was supported in part by National Oceanic and Atmospheric Administration (NOAA)/Office of Oceanic and Atmospheric Research under NOAA-The University of Oklahoma Cooperative through U.S. Department of Commerce under Agreement NA21OAR4320204. (Corresponding author: Valery M. Melnikov.)

Valery M. Melnikov is with the Cooperative Institute for Severe and High-Impact Weather Research and Operations (CIWRO), The University of Oklahoma, Norman, OK 73069 USA, and also with the NOAA/OAR National Severe Storms Laboratory, Norman, OK 73072 USA (e-mail: Valery.Melnikov@noaa.gov).

Eli S. Bridge is with Oklahoma Biological Survey, The University of Oklahoma, Norman, OK 73072 USA (e-mail: ebridge@ou.edu).

Digital Object Identifier 10.1109/LGRS.2024.3375071

radar patterns (Section II). These variations are best explained by the different phases between the horizontally and vertically polarized transmitted waves (Section III). The goal of this study is to assess the significance of this phase for the radar observations of airborne insects.

II. RADAR DATA

WSR-88Ds employ a radar design based on simultaneous transmission of the horizontally and vertically polarized waves [10]. In WSR-88Ds, two channels for these waves are formed on the antenna using a power splitter, two waveguide runs, and a dual-polarization feedhorn. The unequal power split in the channels is accounted for by calibrating Z_{DR} [11], [12]. The measured differential phase (DP) and correlation coefficient (CC) between the polarized waves do not depend on the calibration. The phase shift between the transmitted polarized waves varies among radars, and these variations influence radar variables from nonspherical particles due to interference of the scattered waves [9], [13], [14], [15]. An incident horizontally (H) polarized wave is returned as a mix of horizontally and vertically (V) polarized waves. The latter is called a depolarized wave for the incident H wave. Similarly, two waves originate from an incident V wave. The radar variables depend on the amplitudes and phases of these four waves.

To reduce signal interference between adjacent WSR-88Ds, the radar frequencies are set to different values within a frequency band from 2700 to 2995 MHz (wavelengths from 11.1 to 10.0 cm). These relatively small frequency variations do not affect radar variables from rain; therefore, Z, Z_{DR} , and CC are similar among different radars detecting the same rain events, provided correct radar calibrations are established [5]. The DPs from adjacent radars depend on directions from radars to a sensing rain area, and for non-colocated radars, DPs are typically different because of different signal paths to that area in precipitation. Conversely, radar variables from birds, which are large scatterers at S-band, are affected by frequency deviations because of scattering resonance effects [16]. Insects are Rayleigh scatterers at S-band, and data from closely located radars can separate DP effects.

We examined differences in radar products in two WSR-88Ds located in Norman, Oklahoma: KCRI (frequency of 2995 MHz) and KOUN (2705 MHz), which are separated by 234 m. These radars are research and development systems of the Radar Operations Center and National Severe Storms

1558-0571 © 2024 IEEE. Personal use is permitted, but republication/redistribution requires IEEE permission. See https://www.ieee.org/publications/rights/index.html for more information.

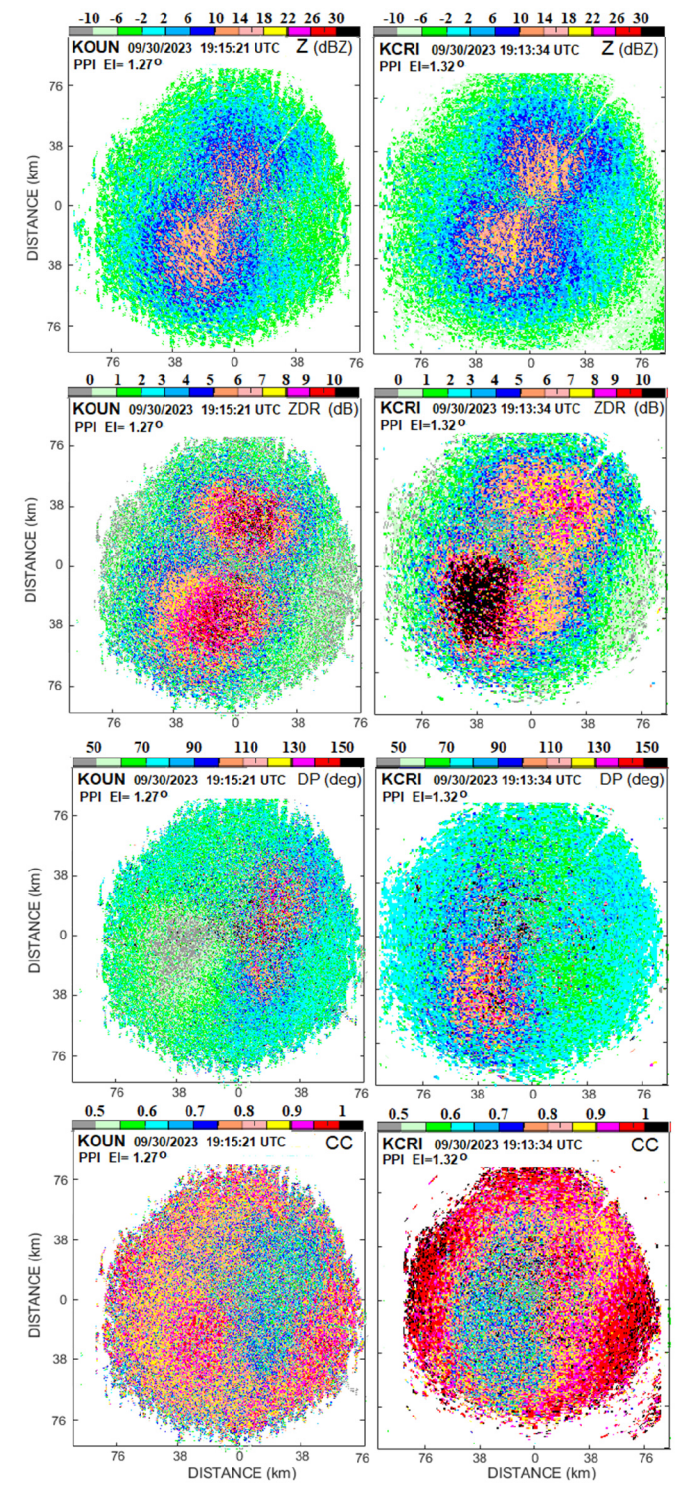


Fig. 1. Radar patterns obtained with WSR-88D (left column) KOUN and (right column) KCRI at an antenna elevation angle of 1.3°. September 30, 2023 at about 1915 UTC.

Laboratory. Outputs from these radars in "clear air" mode often differ. For example, Fig. 1 shows data from migrating insects collected on September 30, 2023. The radars were using scan sequences with three antenna elevation angles common to both: 0.5° , 1.3° , and 1.8° .

One would expect that radar variables from insects simultaneously collected with co-located KOUN and KCRI

would be similar, because insects are Rayleigh scatterers at S-band and alignment of the scatterers is similar for the co-located radars. However, one can see that $Z_{\rm DR}$ patterns from the two radars are noticeably different, and DP and CC fields differ substantially (Fig. 1). The large DP values from KOUN mostly lay in the eastern part of the field, whereas KCRI's image shows higher DP values in its southwestern quadrant. Similarly, the CC patterns from these two radars appear to exhibit an inverse relationship of low values. Since insects are Rayleigh scatterers at S-band, these discrepancies cannot be caused by different radar frequencies. Also, the time lag between the data collection was short (\sim 2 min) and the patterns were observed for several circles of the data collections, i.e., for more than an hour.

III. ANALYSIS OF THE RADAR DATA

To explain the different patterns, we looked to differences in the phases upon transmission between the two radars. The DP upon transmission (DPT) is the phase between transmitted horizontally and vertically polarized radar waves. The antenna, feedhorn, associated waveguides, and the power splitter contribute to the DPT. The first three components are identical on WSR-88Ds, but the phases between horizontally and vertically polarized waves after the power splitter may differ and, therefore, the DPT may differ across radars. The power splitter in WSR-88D produces equal power at its outputs by changing the phases of the waves inside the device. Therefore, the output waves have the same power but may have different phases.

The DPT also depends on the difference in waveguide lengths in the H and V channels and radar frequency. The wavelength λ_w in a waveguide is longer than λ in vacuum (e.g., [17, Sec. 9.12]) $\lambda_w = \lambda/[1 - (f_c/f)^2]^{0.5}$, where f_c and f are the cutoff frequency for the waveguide and radar frequency. For S-band waveguides WR284, $f_c = 2078$ MHz. For KOUN's and KCRI's frequencies $f_1 = 2705$ MHz and $f_2 = 2995$ MHz, the corresponding waveguide wavelengths are $\lambda_{w1} = 17.34$ cm and $\lambda_{w2} = 13.92$ cm. The KOUN's waveguide lengths in the H and V channels are $L_H = 1112.8$ cm and $L_V = 1050.0$ cm including the feedhorn. The number of KOUN's wavelengths in L_H is $L_H/\lambda_{w1} =$ 64.21. The phase difference between the waveguide's input and feedhorn output is $\Phi_H = 0.21 \times 360^\circ = 76.5^\circ$. For the vertically polarized wave, $L_V/\lambda_{w1} = 60.59$ and $\Phi_V =$ $0.59 \times 360^{\circ} = 211.9^{\circ}$. In radar meteorology, the DP is calculated as $\Phi_{DP} = \arg(V_h^* V_v)$ with $V_{h,v}$ being voltages in the channels and * denotes complex conjugate here [10, Sec. 8], i.e., $\Phi_{DP} = \Phi_V - \Phi_H$. Therefore, for KOUN, the contribution to DPT from the different waveguide's lengths is 135.4°. For KCRI, this contribution is $(0.43 - 0.94)360^{\circ} = -183.6^{\circ} =$ 176.4°. So, the different radar frequencies result in different DPT contributions in the identical waveguides.

The H and V WSR-88D's waveguides have adjusting flexible parts, which may result in different signal paths in the channels. A small change in H or V waveguides will result in a substantial change in DPT. For instance, a 1-cm change in the H waveguide at KOUN's frequency, which is 1/17.34 part of

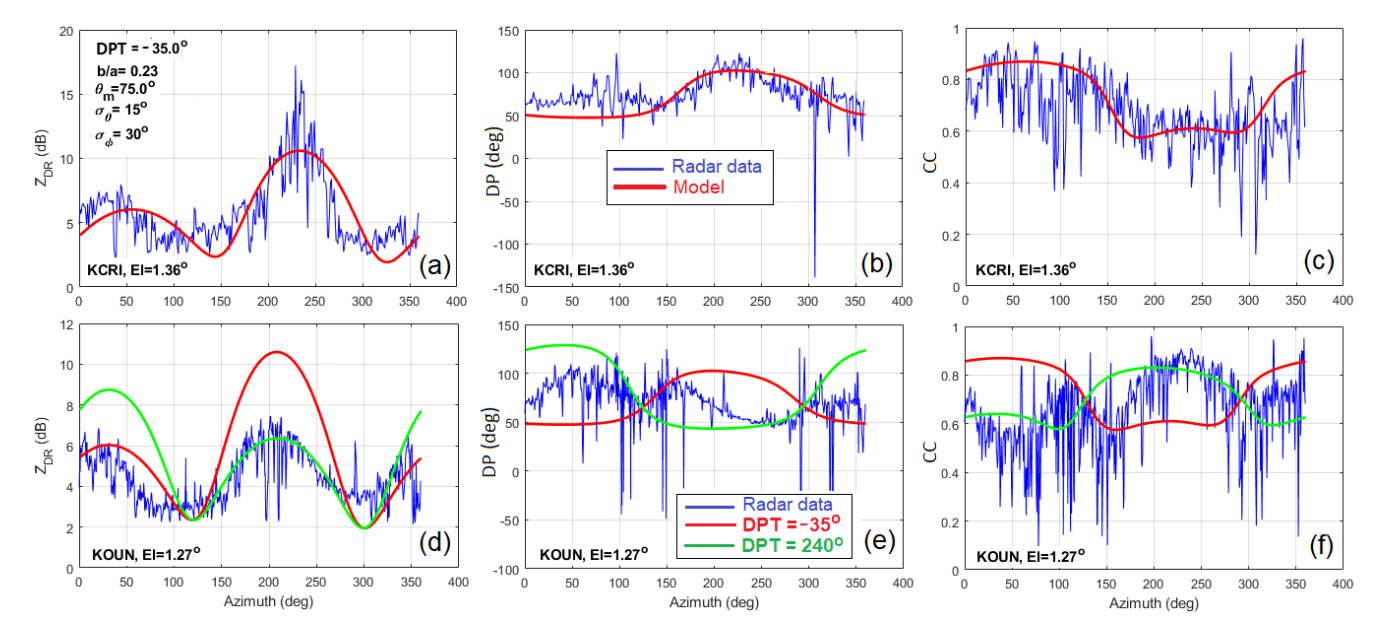


Fig. 2. Radar data from (top) KCRI and (bottom) KOUN are in blue. The red curves in (a)–(c) model results generated using parameters specified in (a). (d)–(f) Model results as green curves for DPT = 240° and red for DPT = -35° . Other parameters in the KOUN simulation are those listed in (a).

 λ_{w1} , equals to 360°/17.34 = 20.8°. These phase uncertainties in the power splitter and waveguides result in the uncertainty in the WSR-88D's DPTs.

To test whether DPT can account for the observed differences, we posed a model of insects as prolate spheroids [9], wherein spheroidal scatterers are characterized by their length (a), width (b), and dielectric permittivity (ε) . The polarimetric properties of Rayleigh scatterers depend on the axis ratio b/a, ε , and orientation of the scatterers relative to the radar beam (e.g., [18, Sec. 2.3.3]). Migrating insects tend to be oriented in a common direction in response to environment's conditions [1]. This direction can be characterized by two angles: 1) the polar angle θ_m between the major scatterer's axis and zenith and 2) the azimuthal angle φ_m relative to North. Horizontally oriented insects flying North have $\theta_m = 90^\circ$ and $\varphi_m = 0^\circ$ ($0 \le \theta_m \le 180^\circ$ and $0 \le \varphi_m \le 360^\circ$; the subscript "m" indicates the mean values). The orientations have distributions with the widths σ_{θ} and σ_{φ} about θ_m and φ_m . Because radar antennas rotate in azimuth, the scatterers appear at various angles relative to the radar beam and the radar variables depend on azimuth. Since insects have nonspherical shapes, the depolarization of scattered waves affects the radar variables, and DPT plays an important role in depolarization [9].

We used the model to determine whether tuning DPT (among other parameters) allows for a reasonable simulation of radar data. We began with an instance of observed data collected by KCRI on September 30, 2023 (\sim 19:15 UTC) in a ring-shaped volume that ranged from 35 to 55 km (comprising 80 radar range gates) with a corresponding height range from 806 to 1267 m above ground level. The radar data were averaged across all range gates within each of 360 azimuths (α) to obtain dependencies $Z_{\rm DR}(\alpha)$, ${\rm DP}(\alpha)$, and ${\rm CC}(\alpha)$. These radar variables do not depend on the concentration of insects but depend on b/a, θ_m , φ_m , σ_θ , σ_φ , and DPT.

The resulting profiles for the 360 azimuths are shown in Fig. 2(a)–(c), with blue lines showing observed data and red lines showing model results. The modeled profiles were obtained by varying the model parameters (including DPT) to subjectively match the KCRI's data. The red curves in Fig. 2(a)–(c) depict the model results for b/a=0.23, DPT = -35° , $\theta_m=75^{\circ}$, $\varphi_m=325^{\circ}$, $\sigma_{\theta}=15^{\circ}$, and $\sigma_{\varphi}=30^{\circ}$. A perfect match between radar and model data was not expected because the model does not precisely represent the true variation in individual body orientations. Nevertheless, it is clear that the obtained model parameters reflect the main features of the radar data.

We further tested the importance of DPT by applying our model to data from KOUN. We used data from the same date and time as before (September 30, 2023, ~19:15 UTC), but because KOUN had a slightly lower scanning angle (1.27° as opposed to 1.32° for KCRI), we used range rings from 36.5 to 57.0 km for KOUN to maintain the same height ranges we used for KCRI (806–1267 m). As before, the observed profiles from KOUN of data averaged across range gates through 360 azimuths are shown as blue curves in Fig. 2(d)–(f). The corresponding model results are shown for two different values of DPT, with all other model parameters held constant. The model with DPT set to 240° [green curves in Fig. 2(d)–(f)] follows the main features of KOUN's observed data. The red curves are for DPT = -35° as in Fig. 2(a)-(c) for KCRI, and they do not follow the main features of the KOUN's data. We can conclude that the difference of DPTs in KCRI and KOUN is about 85°.

The model has a DPT ambiguity of 180° [9]: the range profiles of all radar variables remain the same if θ_m is replaced with $180^{\circ} - \theta_m$ and DPT is replaced with DPT + 180° . The model curves for KCRI radar remain the same for $\theta_m = 105^{\circ}$ and DPT = 145° . For KOUN radar, θ_m should also be 105° because this is a property of the insects. Then, the KOUN's

DPT of 60° matches the radar data. The latter phase equals to a phase of $240^{\circ} + 180^{\circ}$. Therefore, the DPT difference between KOUN and KCRI is 85° in this case. So, the model ambiguity results in the ambiguity of estimated DPTs. For our consideration, it is important that the difference in DPTs remains large and explains the difference in observed radar patterns.

Better DPT estimations could be achieved had our observed data been based on a more uniform distribution of insects. Although the radar and simulated data are not perfectly matched, we have clearly shown that differences in radar patterns can arise due to different DPTs in the radars. An important implication from this result is that DPT can affect the radar variables from nonspherical hydrometeors, such as ice cloud crystals [13], [14]. At S-band, DPT may only weakly affect radar products from rain because raindrops are nearly spherical.

To use polarimetric radar variables from insects quantitatively, the DPT should be measured, and such measurements have not been performed for the WSR-88Ds. A method to obtain DPT for radars capable of sensing in zenith is proposed in [15]. However, WSR-88Ds are not capable of fully vertical sensing—their maximal elevation angle is 60°. Therefore, other methods need to be developed to ascertain DPTs for WSR-88Ds.

IV. CONCLUSION

The differences in polarimetric patterns from insects observed with the two co-located WSR-88Ds are caused by different DPTs in these radars sensing aligned scatterers. Different DPTs can cardinally change radar dual-polarization patterns from airborne insects. To effectively quantify airborne animal activity using dual polarization radar data, DPT should be known. The DPT should also be taken into consideration in an analysis of radar variables from nonspherical hydrometeors, such as ice cloud crystals, snowflakes, and hailstones.

The strong dependence of radar variables on DPT offers the opportunity of getting additional information about scattering media by altering DPT. Such alterations can be achieved with high-power waveguide phase shifters. In dual polarization radars with digital transmitters and phased array radars, DPT can be introduced by a phase delay between generated polarized waves.

ACKNOWLEDGMENT

The authors would like to thank Edwin Dunnavan and the reviewers for their comments, which helped us to improve the presentation.

REFERENCES

- V. A. Drake and D. R. Reynolds, Radar Entomology: Observing Insect Flight and Migration. Boston, MA, USA: CABI, 2012.
- [2] J. Shamoun-Baranes et al., "Meteorological data policies needed to support biodiversity monitoring with weather radar," *Bull. Amer. Meteorol. Soc.*, vol. 102, no. 4, pp. E1234–E1242, 2022, doi: 10.1175/BAMS-D-21-0196.1
- [3] P. Chilson et al., "Partly cloudy with a chance of migration: Weather, radars, and aeroecology," *Bull. Amer. Meteorol. Soc.*, vol. 93, no. 5, pp. 669–686, 2012, doi: 10.1175/BAMS-D-11-00099.1.
- [4] T. Long et al., "Entomological radar overview: System and signal processing," *IEEE Aerosp. Electron. Syst. Mag.*, vol. 35, no. 1, pp. 20–32, Jan. 2020, doi: 10.1109/MAES.2019.2955575.
- [5] J. Zhang et al., "Multi-radar multi-sensor (MRMS) quantitative precipitation estimation: Initial operating capabilities," *Bull. Amer. Meteorolog. Soc.*, vol. 97, no. 4, pp. 621–638, Apr. 2016, doi: 10.1175/bams-d-14-00174.1.
- [6] B. M. Van Doren and K. G. Horton, "A continental system for forecasting bird migration," *Science*, vol. 361, no. 6407, pp. 1115–1118, Sep. 2018, doi: 10.1126/science.aat7526.
- [7] C. Hu, K. Cui, R. Wang, T. Long, S. Ma, and K. Wu, "A retrieval method of vertical profiles of reflectivity for migratory animals using weather radar," *IEEE Trans. Geosci. Remote Sens.*, vol. 58, no. 2, pp. 1030–1040, Feb. 2020, doi: 10.1109/TGRS.2019.2942993.
- [8] P. M. Stepanian and K. G. Horton, "Extracting migrant flight orientation profiles using polarimetric radar," *IEEE Trans. Geosci. Remote Sens.*, vol. 53, no. 12, pp. 6518–6528, Dec. 2015, doi: 10.1109/TGRS.2015.2443131.
- [9] V. M. Melnikov, M. J. Istok, and J. K. Westbrook, "Asymmetric radar echo patterns from insects," *J. Atmos. Ocean. Technol.*, vol. 32, no. 4, pp. 659–674, Apr. 2015, doi: 10.1175/jtech-d-13-00247.1.
- [10] R. J. Doviak and D. S. Zrnic, Doppler Radar and Weather Observations. New York, NY, USA: Academic, 2006.
- [11] D. S. Zrnic, V. M. Melnikov, and J. K. Carter, "Calibrating differential reflectivity on the WSR-88D," *J. Atmos. Ocean. Technol.*, vol. 23, no. 7, pp. 944–951, Jul. 2006, doi: 10.1175/jtech1893.1.
- [12] W. D. Zittel et al., "Use of hydrometeors, Bragg scatter, and sun spikes to determine system ZDR biases in the WSR-88D fleet," in *Proc.* 8th Eur. Conf. Radar Meteorol. Hydrol., 2014. [Online]. Available: http://www.pa.op.dlr.de/erad2014/programme/ExtendedAbstracts/132_ Zittel.pdf
- [13] V. Melnikov, "The impact of the radar differential phase upon transmission on polarimetric variables," in *Proc. 36th AMS Conf. Environ. Inf. Process. Technol.*, 2020. [Online]. Available: https://ams.confex.com/ams/2020Annual/meetingapp.cgi/Paper/363409
- [14] V. Melnikov, "Impacts of the phase shift between incident radar waves on the polarization variables from ice cloud particles," *J. Atmos. Ocean. Technol.*, vol. 37, no. 8, pp. 1423–1436, Aug. 2020, doi: 10.1175/jtech-d-19-0197.1.
- [15] D. S. Zrnić and V. M. Melnikov, "Estimation of transmitted differential phase on dual-polarization radars," *J. Atmos. Ocean. Technol.*, vol. 40, no. 10, pp. 1221–1239, Oct. 2023, doi: 10.1175/jtech-d-22-0014.1.
- [16] V. M. Melnikov, R. R. Lee, and N. J. Langlieb, "Resonance effects within S-band in echoes from birds," *IEEE Geosci. Remote Sens. Lett.*, vol. 9, no. 3, pp. 413–416, May 2012, doi: 10.1109/LGRS.2011. 2169933.
- [17] D. T. Paris and F. K. Hurd, Basic Electromagnetic Theory. New York, NY, USA: McGraw-Hill, 1969.
- [18] V. N. Bringi and V. Chandrasekar, Polarimetric Doppler Weather Radar: Principles and Applications. Cambridge, U.K.: Cambridge Univ. Press, 2001.